Pergamon

Int. J. Solids Structures Vol. 35, Nos. 3–4, pp. 205–217, 1998

0020-7683/98 $19.00 + .00

PII: S0020-7683(97)00063-2

MIXED MODE FRACTURE IN EPICYCLOID SPECIMENS II. POINT FORCE LOADING

W. H. MÜLLER
Laboratorium für Technische Mechanik, FB 10, Universität-Gesamthochschule-Paderborn, Pohlweg 47-49, 33098 Paderborn, Germany

H. GAO
Division of Mechanics and Computation, Durand Building, Stanford University, Stanford, CA 94305, U.S.A.

(*Received* 15 *October* 1996; *in revised form* 22 *January* 1997)

Abstract—The method of complex potentials is used to obtain an analytical solution for the stresses in epicycloidal specimens due to point force loading. The solution is used to obtain an analytical expression for the stress intensity factors of cusp-like cracks in such specimens which can be considered as a generalization of the well-established concept of Griffith cracks. It is shown that by suitable positioning of the point forces negative mode I stress intensity factors will result. This illustrates the potential of epicycloid specimens for the determination of fracture properties under compressive loading where frictional contact of the crack surfaces is a priori avoided. © 1997 Elsevier Science Ltd.

1. EPICYCLOID SPECIMENS AND FRACTURE MECHANICS

In a recent paper by Gao *et al.* (1997) the potential of epicycloid specimens for experimental determination of interface fracture properties as well as testing under compressive loading conditions has been explored. It was demonstrated that epicycloid specimens contain defects in the form of *cusps* which can be considered as a generalization of the traditional concept of a Griffith crack. So far only the effects of thermo-mechanical loads (induced by a "hot spot" region) have been studied. In the present paper, the concept of epicycloid fracture specimens will be extended to include the influence of purely mechanical loading by means of point forces.

The generic mapping of the cycloid family can be written as follows [Bronstein and Semendjajew (1976); Mushkhelishvili (1963)]:

$$z = \omega(\zeta) = R\left(\zeta - \frac{\varepsilon}{n+1}\zeta^{n+1}\right), \quad \zeta = \exp(\mathrm{i}\vartheta), \quad R = (n+1)\rho \tag{1}$$

where $z = x + \mathrm{i}y$ denotes the position vector in the original complex plane, $n \in \mathrm{IN}$, $\vartheta \in [0, 2\pi]$, $\varepsilon \in [0, 1]$ and ρ is the radius of the revolving circle. In particular the choice $\varepsilon = 1$ leads to epicycloids exhibiting the characteristic feature of *cusp-like cracks*. Figure 1(a) shows an epicycloid with one cusp, i.e. the case where $n = 1$†, which is also known as *Pascal's limaçon*. As indicated in the figure the specimen is subjected to self-equilibrating point forces. Clearly, this type of loading is analogous to three point bending of a straight bar that contains an edge crack of the Griffith-type: Fig. 1(b).

The following analysis of the stresses and the stress intensify factors focuses on the case $n = 1$, i.e. on epicycloid specimens of the Pascal's limaçon type subjected to self-equilibrating point forces (Fig. 2). However, the analysis will be presented such that it can easily be extended to cover other cases in which $n > 1$. It will be shown that the finite geometry of epicycloid specimens allows to obtain *analytical* solutions. These can easily be evaluated numerically even if their explicit mathematical form generally proves to be quite

† The radius ρ was chosen to be equal to 1.

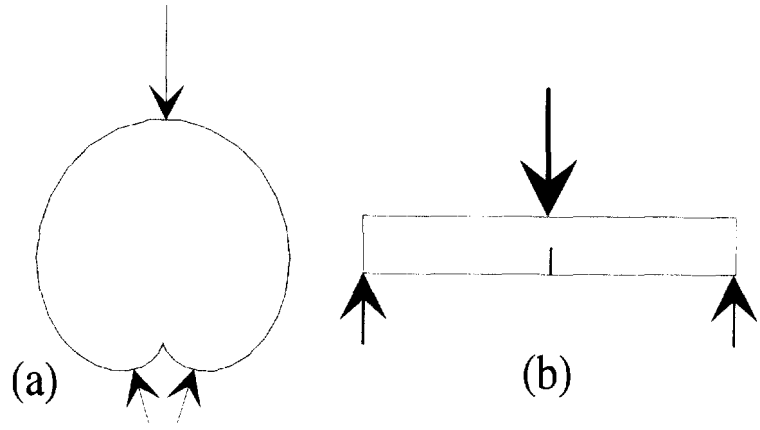

Fig. 1. (a) Epicycloid specimen subjected to point forces vs (b) classical three point bending jig.

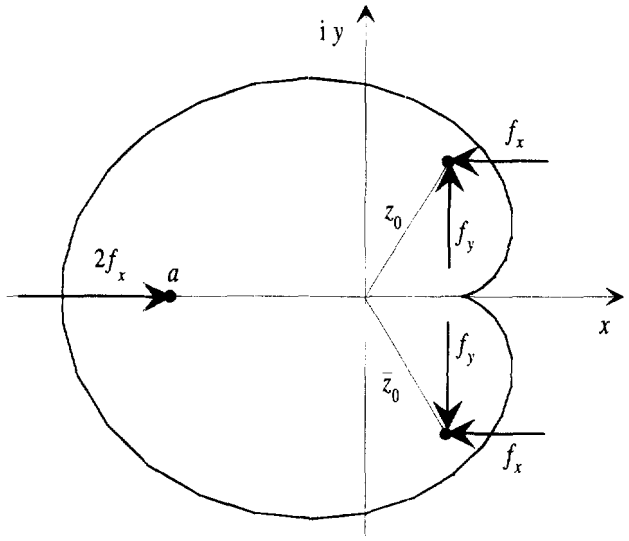

Fig. 2. Pascal's limaçon subjected to self-equilibrating point forces in horizontal and vertical direction.

unwieldy. It should be noted that in contrast to epicycloid specimens the mathematical expressions for the stress intensity factors of straight notched bending bars are generally expressed by "empirical formulae" which are based on numerical analyses such as boundary collocation or finite element methods [Tada *et al.* (1985)].

2. STRESS ANALYSIS

2.1. *A reminder of complex stress analysis*

Following the concepts of two-dimensional theory of elasticity in complex variable notation the resultant force, F, acting on a line, L, can be computed from

$$F(z) = -\mathrm{i}[\varphi(\tilde{z}) + \tilde{z}\overline{\varphi'(\tilde{z})} + \overline{\psi(\tilde{z})}]_{\tilde{z}=a}^{\tilde{z}=z}, \quad \forall z \in L, \tag{2}$$

where $[\ ]_{\tilde{z}=a}^{\tilde{z}=z}$ denotes the increase undergone by the expression in brackets as the point $\tilde{z}$ passes along the line L from points a to z. Moreover, $\varphi(z)$ and $\psi(z)$ denote the complex stress potentials of the Mushkhelishvili–Kolosov equations [e.g. Sokolnikoff (1956); Muskhelishvili (1963)]:

$$\sigma_{22}+\sigma_{11} = 2[\varphi'(z)+\overline{\varphi'(z)}]$$
$$\sigma_{22}-\sigma_{11}+2\mathrm{i}\sigma_{12} = 2[\bar{z}\varphi''(z)+\psi'(z)] \tag{3}$$

and σ_{ij}, $i, j \in \{1,2\}$ are the stresses in rectangular coordinates. In the case of a stress-free boundary, such as the periphery of the epicycloid specimen shown in Fig. 2, it is necessary and sufficient that the resultant force, F, vanishes in each and every point, z, on the periphery. Therefore:

$$\varphi(z)+z\overline{\varphi'(z)}+\overline{\psi(z)} = 0, \quad \forall z \in L. \tag{4}$$

2.2. *Determination of the stress potentials*

Similarly to the procedure presented in the paper by Gao *et al.* (1997) the stress potentials, $\varphi(z)$ and $\psi(z)$, are divided into two parts as follows:

$$\varphi(z) = \varphi_\infty(z)+\varphi_s(z), \quad \psi(z) = \psi_\infty(z)+\psi_s(z). \tag{5}$$

The first part, identified by the subscript "∞", refers to the complex potentials that characterize the stresses produced by point forces in an *infinite plane*. For a single point force, (X, Y), located at an arbitrary position z_0 in the complex plane it can be shown that [Muskhelishvili (1963), Section 57]:

$$\varphi_\infty(z) = -\frac{X+\mathrm{i}Y}{2\pi(1+\kappa)}\ln(z-z_0)+\varphi_0 \tag{6}$$

and

$$\psi_\infty(z) = \frac{\kappa(X-\mathrm{i}Y)}{2\pi(1+\kappa)}\ln(z-z_0)+\frac{\bar{z}_0(X+\mathrm{i}Y)}{2\pi(1+\kappa)}\frac{1}{z-z_0}+\psi_0, \quad \kappa = \begin{cases} 3-4\nu, & \text{plane strain} \\ \dfrac{3-\nu}{1+\nu}, & \text{plane stress} \end{cases} \tag{7}$$

where φ_0 and ψ_0 refer to functions that are holomorphic near the point z_0 and ν denotes Poisson's ratio.

Consequently, for the three point forces shown in Fig. 2, which are located at positions z_0, $\bar{z}_0$, a, it can easily be established that:

$$\varphi_\infty(z)/A = \ln\frac{(z-z_0)(z-\bar{z}_0)}{(z-a)^2}-\mathrm{i}\frac{f_y}{f_x}\ln\frac{z-z_0}{z-\bar{z}_0} \tag{8}$$

and

$$\psi_\infty(z)/A = -\kappa\ln\frac{(z-z_0)(z-\bar{z}_0)}{(z-a)^2}-\mathrm{i}\kappa\frac{f_y}{f_x}\ln\frac{z-z_0}{z-\bar{z}_0} + \frac{2a}{z-a}-\frac{\bar{z}_0}{z-z_0}-\frac{z_0}{z-\bar{z}_0}+\mathrm{i}\frac{f_y}{f_x}\left(\frac{\bar{z}_0}{z-z_0}-\frac{z_0}{z-\bar{z}_0}\right) \tag{9}$$

with

$$A = \frac{f_x}{2(1+\kappa)} \tag{10}$$

where all holomorphic parts have been neglected.

The second set of functions in eqn (5), identified by the subscript "s", must be chosen such that eqn (4) is satisfied, i.e.

$$\varphi_s(z)+z\overline{\varphi_s'(z)}+\overline{\psi_s(z)} = -\varphi_\infty(z)-z\overline{\varphi_\infty'(z)}-\overline{\psi_\infty(z)}, \quad \forall z\in L. \tag{11}$$

It is advantageous to evaluate this condition on the unit circle. To this end use is made of the conformal mapping shown in eqn (1) which for $n = 1$, $\varepsilon = 1$ can be written as follows:

$$z = \frac{R}{2}\zeta(2-\zeta). \tag{12}$$

Moreover, since the potentials φ_s and ψ_s are analytical within the unit circle they can be represented by power series as follows

$$\varphi_s(\zeta) = \sum_{m=1}^{\infty} a_m\zeta^m, \quad \psi_s = \sum_{m=1}^{\infty} b_m\zeta^m \tag{13}$$

if rigid body displacements are ignored. Application of the Cauchy operator:

$$\frac{1}{2\pi i}\oint_{|\zeta|=1}\frac{(\cdot)\,d\zeta}{\zeta-\eta}, \quad \forall|\eta|\leqslant 1 \tag{14}$$

to the left-hand side (LHS) of eqn (11) leads to:†

$$\frac{1}{2\pi i}\oint_{|\zeta|=1}\frac{\text{LHS}\,d\zeta}{\zeta-\eta} = \sum_{m=1}^{\infty} a_m\eta^m + \frac{1}{2}\bar{a}_1\eta - \frac{1}{2}(\bar{a}_1\eta^2+2\bar{a}_2\eta)$$

$$\equiv \varphi_s(\eta)+\frac{1}{2}\bar{a}_1\eta-\frac{1}{2}(\bar{a}_1\eta^2+2\bar{a}_2\eta). \tag{15}$$

In order to determine the coefficients a_1 and a_2 the Cauchy operator shown in eqn (14) is now applied to the various terms shown on the right-hand side (RHS) of eqn (11). By means of Cauchy's theorem it can be shown that:

$$-\frac{1}{A}\frac{1}{2\pi i}\oint_{|\zeta|=1}\frac{\varphi_\infty(\zeta)\,d\zeta}{\zeta-\eta} = -\ln\frac{(2-\eta-\zeta_0)(2-\eta-\bar{\zeta}_0)}{(2-\eta-\alpha)^2}+i\frac{f_y}{f_x}\ln\frac{2-\eta-\zeta_0}{2-\eta-\bar{\zeta}_0} \tag{16}$$

and similarly

$$-\frac{1}{A}\frac{1}{2\pi i}\oint_{|\zeta|=1}\frac{(z\overline{\varphi_\infty'(z)}+\overline{\psi_\infty(z)})\,d\zeta}{\zeta-\eta} = \kappa\ln\frac{(1-\zeta_0\eta)(1-\bar{\zeta}_0\eta)}{(1-\alpha\eta)^2}-i\kappa\frac{f_y}{f_x}\ln\frac{1-\bar{\zeta}_0\eta}{1-\zeta_0\eta}-$$

$$\oint_{|\zeta|=1}\frac{(G(\zeta,\zeta_0)+G(\zeta,\bar{\zeta}_0)-2G(\zeta,\alpha)+if_y/f_x[G(\zeta,\zeta_0)-G(\zeta,\bar{\zeta}_0)])\,d\zeta}{\zeta-\eta} \tag{17}$$

where the following contraction has been used

$$G(x,t) = \frac{(x-t)(2-x-t)}{\left(\frac{1}{x}-\bar{t}\right)\left(2-\frac{1}{x}-\bar{t}\right)} \tag{18}$$

and quantities ζ_0, α are obtained from eqn (12), i.e.

† see Gao *et al.* (1997) for further details of the proof for arbitrary values of n and ε.

$$z_0 = \frac{R}{2}\zeta_0(2-\zeta_0), \quad a = \frac{R}{2}\alpha(2-\alpha). \tag{19}$$

The remaining Cauchy integrals of eqn (17) were solved with Mathematica® by application of the residue theorem. Next the results shown in eqns (16) and (17) were expanded in terms of the variable η to identify the coefficients λ_1 and λ_2 in the following series:

$$-\frac{1}{A}\frac{1}{2\pi i}\oint_{|\zeta|=1}\frac{\mathrm{RHS}\,d\zeta}{\zeta-\eta} = \sum_{i=1}^{\infty}\lambda_i\eta^i. \tag{20}$$

Since the explicit mathematical form of these coefficients is quite unwieldy they will not be explicitly presented in this paper. However, it should be noted that both coefficients turn out to be *real* quantities. By comparison of eqn (20) with eqn (15) the following relations for the unknown coefficients a_1 and a_2 are obtained:

$$a_1 + \frac{1}{2}\bar{a}_1 - \bar{a}_2 = \lambda_1, \quad a_2 - \frac{1}{2}\bar{a}_1 = \lambda_2 \tag{21}$$

from which the real parts can be determined

$$\mathrm{Re}\,a_1 = \lambda_1 + \lambda_2, \quad \mathrm{Re}\,a_2 = \frac{1}{2}(\lambda_1 + 3\lambda_2). \tag{22}$$

In fact, it is sufficient to determine the real parts of these coefficients since their imaginary parts contribute only to a rigid body rotation which will be suppressed. That is, it will be assumed that the unknown coefficients a_1, a_2 are given as follows:

$$a_1 = \mathrm{Re}\,a_1 + i\,\mathrm{Im}\,a_1, \quad a_2 = \mathrm{Re}\,a_2 + i\,\mathrm{Im}\,a_2. \tag{23}$$

Then by insertion into the first of eqn (13) it follows that:

$$\varphi_s = \mathrm{Re}\,a_1\zeta + i\,\mathrm{Im}\,a_1\frac{z}{R} + \left(a_2 - i\frac{\mathrm{Im}\,a_1}{2}\right)\zeta^2 + a_3\zeta^3 + \ldots \tag{24}$$

where eqn (12) has been used. Recall the general expression for the rotation, ε [e.g. Muskhelishvili (1963), Section 36]:

$$\varepsilon = \frac{1+\kappa}{2\mu}\cdot\frac{\varphi'(z) - \overline{\varphi'(z)}}{2i} \tag{25}$$

where μ denotes the shear modulus and it becomes clear that in order to avoid a rigid body rotation it is required that:

$$\mathrm{Im}\,a_1 = 0 \tag{26}$$

and, consequently, by virtue of eqn (21)

$$\mathrm{Im}\,a_2 = 0. \tag{27}$$

By the combination of eqns (5), (8), (9), (17) and (18) it finally follows for the complex potential $\varphi(z)$:

$$\frac{1}{A}\varphi(\eta) = \ln\frac{(\eta-\zeta_0)(\eta-\overline{\zeta_0})}{(\eta-\alpha)^2} - \mathrm{i}\frac{f_y}{f_x}\ln\frac{\eta-\zeta_0}{\eta-\bar{\zeta}_0} + \kappa\ln\frac{(1-\eta\zeta_0)(1-\eta\overline{\zeta_0})}{(1-\eta\alpha)^2} - \mathrm{i}\kappa\frac{f_y}{f_x}\ln\frac{1-\eta\overline{\zeta_0}}{1-\eta\zeta_0} -$$
$$\oint_{|\zeta|=1}\frac{(G(\zeta,\zeta_0)+G(\zeta,\bar{\zeta}_0)-2G(\zeta,\alpha)+\mathrm{i}f_y/f_x[G(\zeta,\zeta_0)-G(\zeta,\bar{\zeta}_0)])\,\mathrm{d}\zeta}{\zeta-\eta} - \frac{1}{2}\bar{a}_1\eta + \frac{1}{2}(\bar{a}_1\eta^2+2\bar{a}_2\eta). \tag{28}$$

Analogously to the procedure described in Gao *et al.* (1997) this result can now be used to retrieve the second potential $\psi(z)$ directly from eqn (11).

2.3. *Stress intensity factors for the cusp in a Pascal's limaçon specimen*

The stress intensity factors (SIFs), K_I and K_II, of a cusp in a epicycloid can be determined from the following asymptotic form for the complex potential [see Gao *et al.* (1997)]:

$$K_\mathrm{I} - \mathrm{i}K_\mathrm{II} = -\lim_{z\to 0}\{2\sqrt{-2\pi z_\mathrm{c}}\varphi'(z_\mathrm{c})\} \tag{29}$$

where z_c denotes a complex vector originating at the tip of the cusp. Performing the limit yields for an epicycloid specimen of the Pascal's limaçon type

$$K_\mathrm{I} - \mathrm{i}K_\mathrm{II} = 2\sqrt{\frac{\pi}{R}}\varphi'(\zeta = 1). \tag{30}$$

3. RESULTS AND DISCUSSION

Figure 3 presents the SIFs obtained from numerical evaluation of eqns (28) and (30) for the case $f_y/f_x = 0$ for all possible positions $z_0 = x_0 + \mathrm{i}y_0$ of horizontal forces (Fig. 2). Due to the symmetry of the problem, only a mode I component of the SIFs exist which was normalized by:

$$K_0 = A\sqrt{\frac{2}{R}}. \tag{31}$$

Two regions of different K_I-sign are distinctly visible. If the horizontal forces are positioned toward the interior of the Pascal's limaçon, the SIFs become negative. On the other hand, if they are located at the outer regions, K_I becomes positive. This behavior must be attributed to the signs of the moments which are exerted on the cusp through the horizontal point forces. If the two horizontal forces are arranged relatively close to the symmetry line the resulting moment is negative resulting in closure of the cusp and vice versa. Clearly, negative and positive regions must be separated by a line of "blind spots" where positioning of forces results in vanishing SIFs as will be discussed in more detail below.

It should be noted that the SIFs along the symmetry line, i.e. on the real axis $z_0 = x_0$, are purely negative. Numerical values can be obtained from the following equation†:

$$\frac{K_\mathrm{I}}{K_0} = \sqrt{2\pi}\frac{1+\zeta_0}{1-\zeta_0}(2+\kappa-[5-2\kappa]\zeta_0+2[1-\kappa]\zeta_0^2), \quad \zeta_0 = 1-\sqrt{1-\frac{x_0}{\rho}} \tag{32}$$

which is valid for arbitrary choice of f_y/f_x. Figure 4 shows a graphical representation of this result. It is noteworthy that the SIF goes to minus infinity if point forces move toward the tip of the cusp and to zero if all horizontal forces meet at $\zeta_0 = -1$.

The location and shape of the line of blind spots as well as the size and intensity of the regions of positive or negative K_I is affected by the relative strength of point forces in

† which was obtained through symbolic evaluation of eqns (28) and (30) by means of Mathematica®.

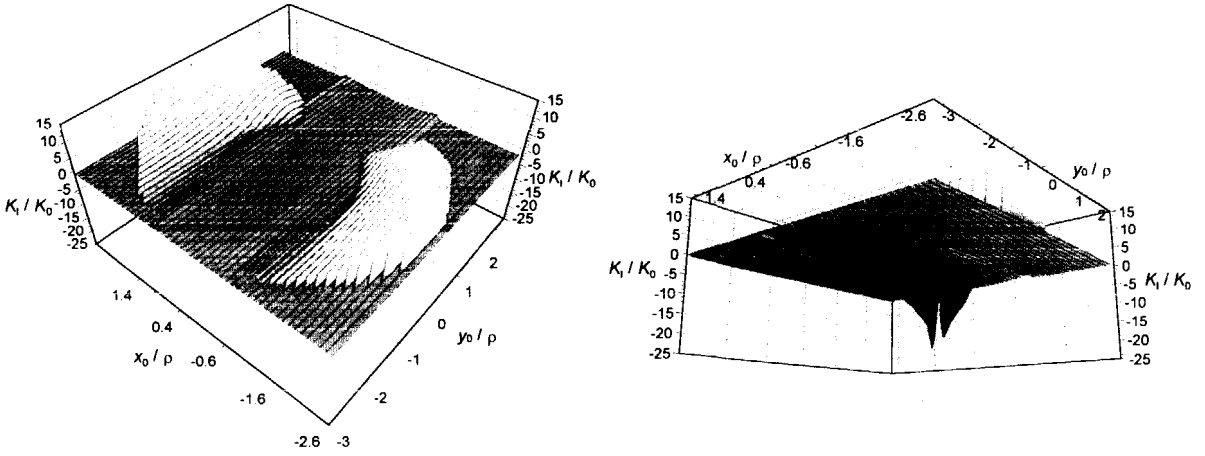

Fig. 3. Top and bottom view of SIFs for $f_y/f_x = 0$ for all possible positions z_0 within Pascal's limaçon.

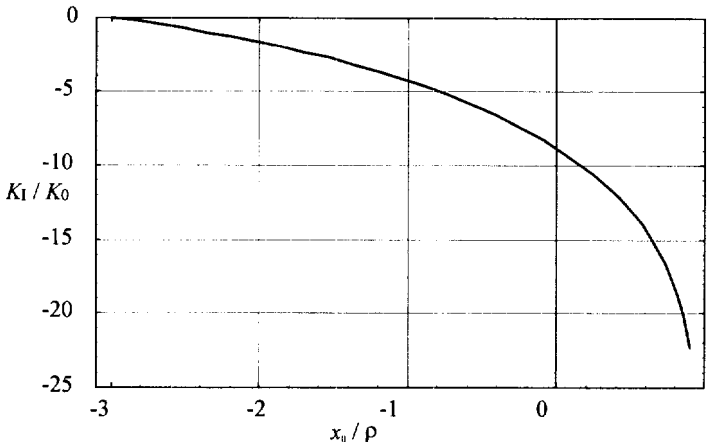

Fig. 4. Negative SIFs along the axis of symmetry of Pascal's limaçon.

vertical direction, in other words by the factor f_y/f_x. Figures 5 and 6 show the SIF resulting from the choice $f_y/f_x = \pm 0.5$. As one would expect intuitively positive values of f_y/f_x reduce the zone of negative K_1 and vice versa. This is more closely examined in Fig. 7 in which lines of blind spots for $f_y/f_x \neq 0$ are juxtaposed to the one for $f_y/f_x = 0$. It was mentioned before and explicitly shown in eqn (32) that the SIF for the point $\zeta_0 = -1 \Rightarrow x_0 = -3R$ is always equal to zero independently of the value chosen for $f_y/f_x = \pm 0.5$. In other words, this point is part of every line of blind spots. However, this is not clearly visible in some of the pictures shown in Fig. 7 and should be kept in mind.

Figure 8 shows the behavior of SIFs when evaluated along the imaginary axis for different values of f_y/f_x. The previous remarks hold accordingly.

Figure 9 presents a device which allows to simply realize three point bending of an epicycloid specimen of the Pascal's limaçon type: a smooth cylinder, situation (a), or a wedge, situation (b), are pressed against the cusp. This leads to normal loading conditions on the surface of the specimen depending upon the diameter, $2r$, of the inserted cylinder or of the angle, α, of the wedge. The SIFs corresponding to this type of loading are shown in Fig. 10. They were calculated by using the following expression for f_y/f_x:

$$\frac{f_y}{f_x} = \frac{\dot{x}_0}{\dot{y}_0} = \frac{\mathrm{Im}(\zeta_0[\zeta_0 - 1])}{\mathrm{Re}(\zeta_0[1 - \zeta_0])}, \quad \zeta_0 = \exp(\mathrm{i}\vartheta) \tag{33}$$

where the dot refers to differentiation with respect to ϑ. This equation follows from eqn (1) for $n = 1$, $\varepsilon = 1$ and it guarantees normal loading conditions. Note that for $\vartheta = 60°$ i.e. for clamping the epicycloid between two parallel plates, the SIFs change from positive to negative values. This agrees with intuition as well as with previous remarks according to which a negative value of f_y/f_x tends to promote fracture under compression. Furthermore, it should be noted that the SIFs tend to $+\infty$ and $-\infty$ for $\vartheta = 0°$ and $120°$, respectively. This is not surprising since in the first case a singular force is applied directly at the tip of the cusp and in the second case loading in vertical direction becomes infinitely large in order to satisfy eqn (33).

Figure 11 allows to obtain the radius, r of the inserted cylinder shown in Fig. 9 when normalized by the "epicycloid radius", R. The viewgraph is a consequence of the following analytical reaction which results from simple geometrical considerations:

$$\frac{r}{R} = -\frac{\left(\sin\vartheta - \frac{1}{2}\sin(2\vartheta)\right)\sqrt{2(1-\cos\vartheta)}}{\sin\vartheta - \sin(2\vartheta)} \tag{34}$$

Note that this ratio goes to $\pm\infty$ if the angle ϑ approaches $60°$ from below or above, as it should, since this describes the case of clamping a Pascal's limaçon between two parallel

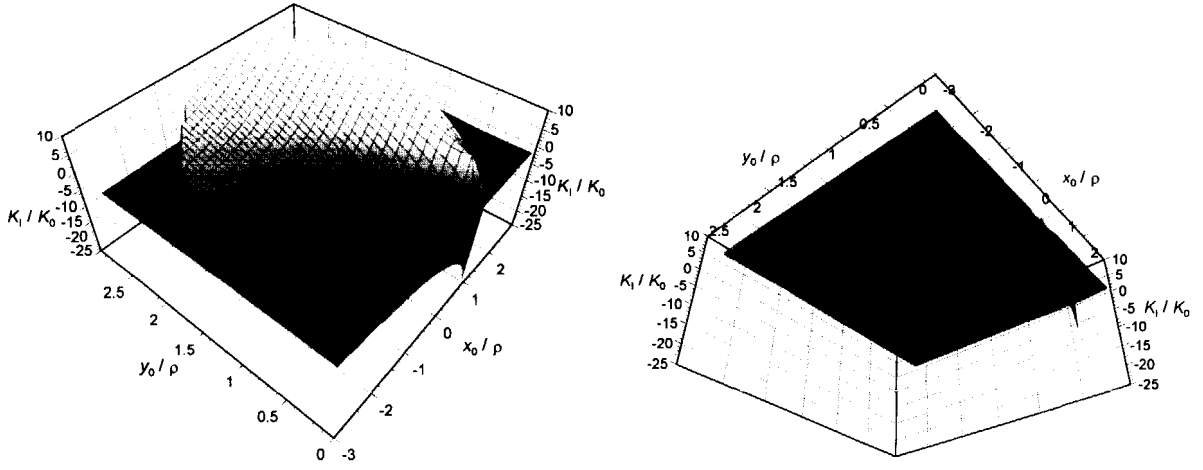

Fig. 5. Top and bottom view of SIFs for $f_y/f_x = +0.5$ for all possible positions z_0 within one half of Pascal's limaçon.

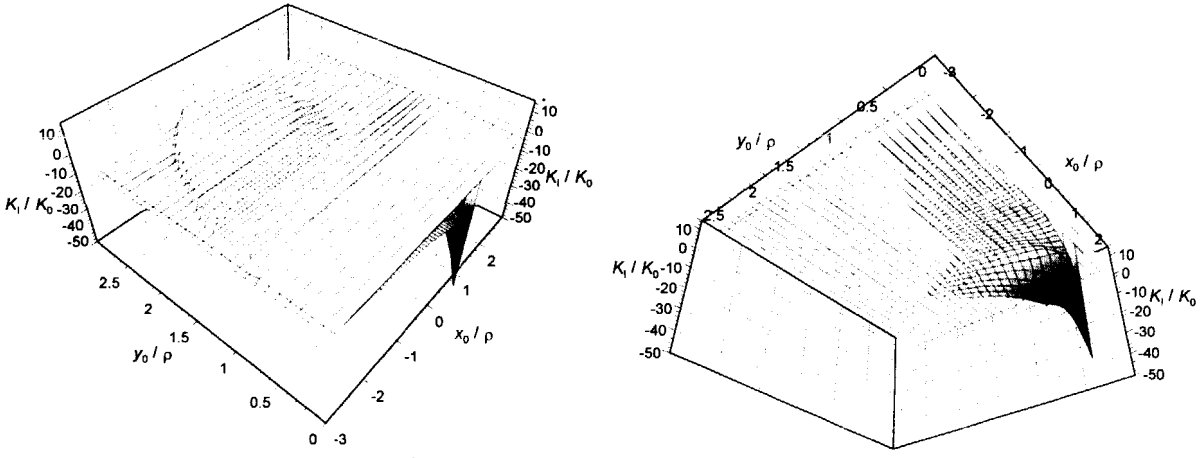

Fig. 6. Top and bottom view of SIFs for $f_y/f_x = -0.5$ for all possible positions z_0 within one half of Pascal's limaçon.

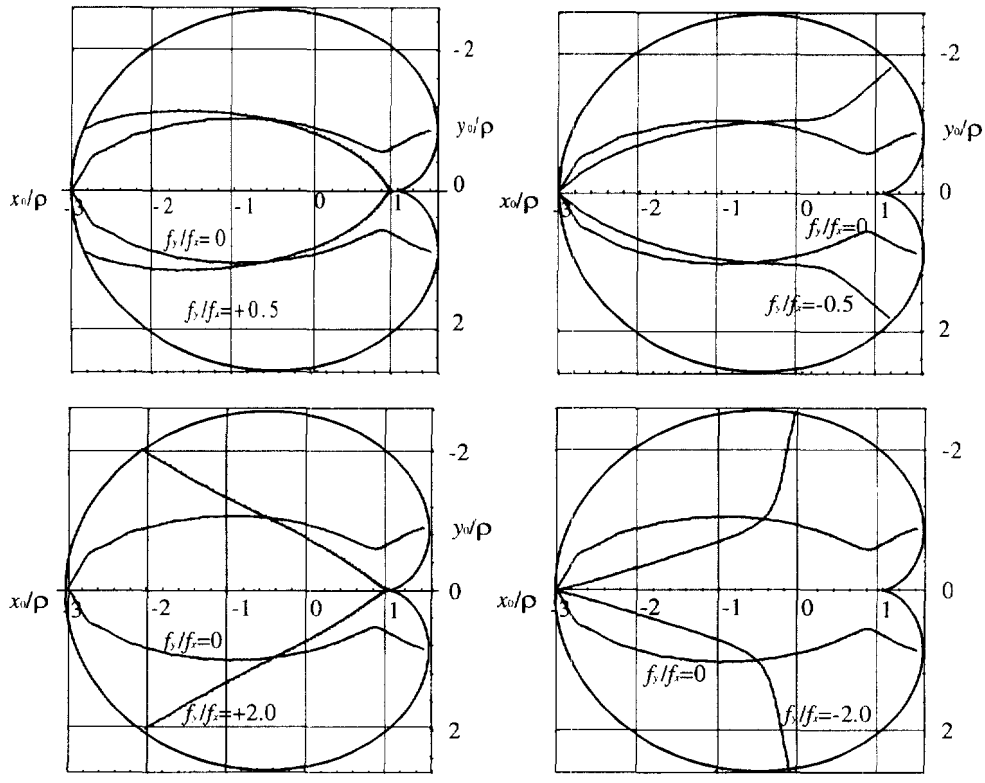

Fig. 7. Lines of blind spots for $f_y/f_x = +0.5$, -0.5, $+2.0$ and -2.0 in comparison with the line of blind spots for $f_y/f_x = 0$.

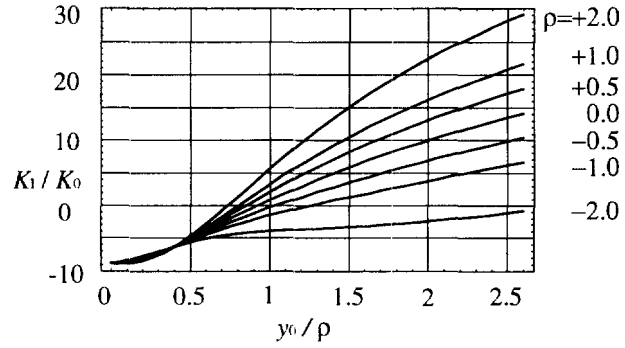

Fig. 8. SIFs along the imaginary axis for $f_y/f_x = \pm 0.5$, ± 1.0, ± 2.0 and 0.0.

plates. Negative values of r/R correspond to pressing the epicycloid onto the inner surface of a hollow cylinder.

Figure 12 shows the wedge angle, α, of Fig. 9 as a function of the mapping angle ϑ. The plot is based on the following relation which, again, can be obtained by geometrical analysis:

$$\alpha = -\arctan\frac{\cos\vartheta - \cos(2\vartheta)}{\sin\vartheta - \sin(2\vartheta)} = \frac{3\vartheta}{2}. \tag{35}$$

Finally, Fig. 13 presents the SIFs obtained for purely horizontal loading of the surface of an epicycloid specimen of the Pascal's limaçon type, i.e. when $f_y/f_x = 0$. Analogously to the result presented in Fig. 10 for loading conditions normal to the surface the SIFs change sign at $\vartheta = 60°$. However, in contrast to the former results negative SIFs result at angles smaller than this value and vice versa which also agrees with intuition (negative = closing bending movements at small angles and positive = opening bending moments for large

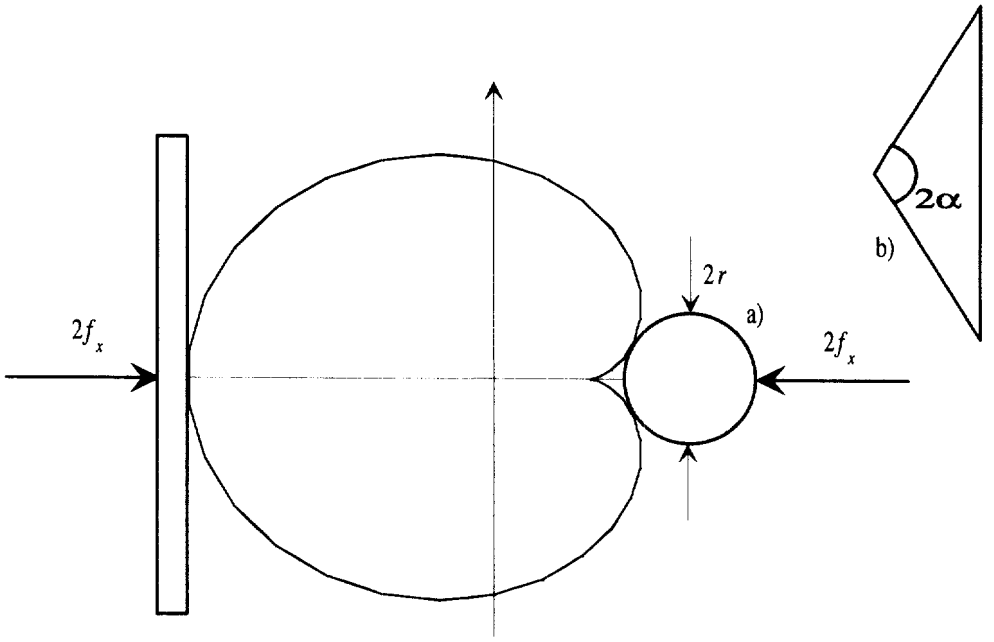

Fig. 9. Realization of a three point bending jig by using epicycloid specimens.

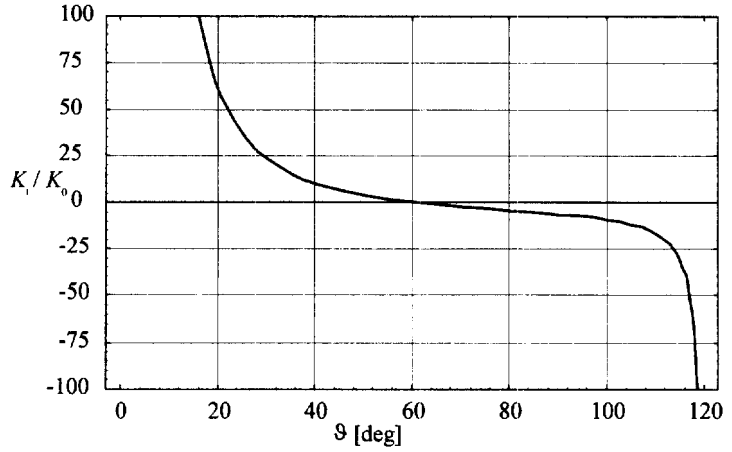

Fig. 10. SIFs for loading conditions normal to the surface of an epicycloid of the Pascal's limaçon type.

angles). Furthermore note that the SIF assumes a maximum value at $\approx 105^\circ$ which can be interpreted as the optimum of the opening moment.

6. CONCLUSIONS

The intent of this paper is to draw attention to the potential of epicycloid specimens in fracture mechanics testing. To this end an analytical solution for the stresses in such specimens is derived, based on complex potential theory and specialized to the case self-equilibrating point forces applied to an epicycloid of the Pascal's limaçon type. The solution is used to derive analytical expressions for the mode I stress intensity factor of the cusp-like crack in that specimen. This solution is numerically evaluated for various position of the applied point forces. It is demonstrated by the calculated values that strongly negative

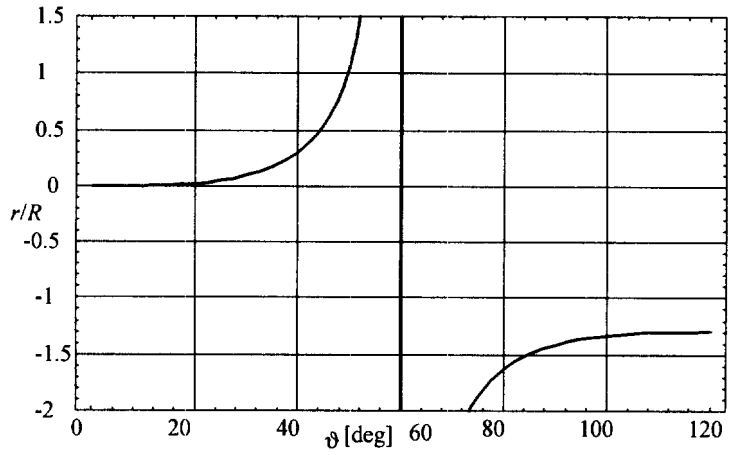

Fig. 11. Normalized radius, r/R, of the inserted cylinder as a function of mapping angle, ϑ.

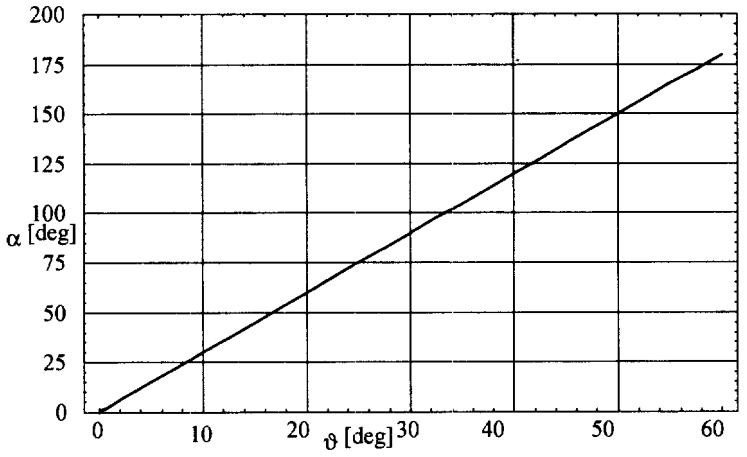

Fig. 12. Wedge angle, α, as a function of mapping angle, ϑ.

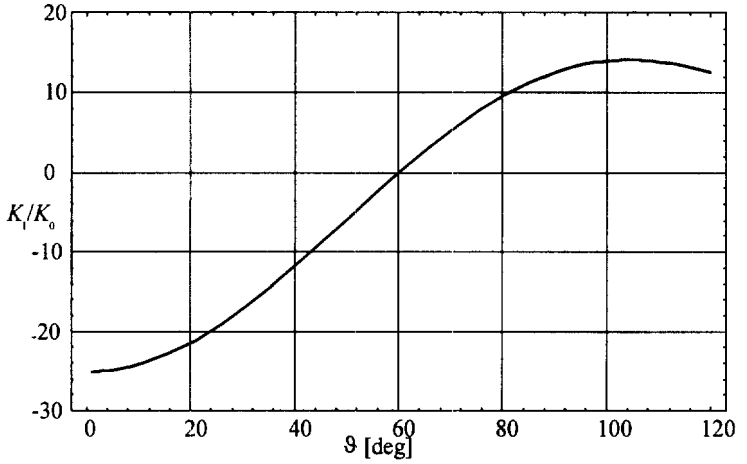

Fig. 13. SIFs for horizontal loading conditions on the surface of an epicycloid of the Pascal's limaçon type.

K_I-conditions can be enforced without frictional contact and shear of the crack surfaces when the point forces take suitable positions.

Acknowledgements—The foundation to this paper was laid during a sabbatical visit of one of the authors (H.G.) to the Universität-Gesamthochschule-Paderborn at the beginning of 1996. The stay was financially supported by the Kommission für Forschung und wissenschaftlichen Nachwuchs der Universität Paderborn. This support is

gratefully acknowledged. The authors would also like to thank the head of the Laboratorium für Technische Mechanik, o. Professor Dr rer. nat. K.P. Herrmann, for his hospitality and support.

REFERENCES

Bronstein, I. N. and Semendjajew, K. A. (1976) *Taschenbuch der Mathematik*, 16. Auflage. Verlag Harri Deutsch, Zürich, Frankfurt/Main, Thun.

Gao, H., Müller, W. H. and Kemmer, G. (1997) Mixed mode fracture in epicycloid specimens I. Thermal inclusions. *International Journal of Solids and Structures* (accepted).

Muskhelishvili, N. I. (1963) *Some Basic Problems of the Mathematical Theory of Elasticity*, 4th edn, Noordhoff, Groningen, Netherlands.

Sokolnikoff, I. S. (1956) *Mathematical Theory of Elasticity*, 2nd edn. McGraw-Hill, New York.

Tada, H., Paris, P. C. and Irwin, G. R. (1985) *The Stress Analysis of Cracks Handbook*. Del Research Corporation, St Louis, Missouri.